The Analysis of Image Contrast: From Quality Assessment to Automatic Enhancement

Ke Gu, Guangtao Zhai, *Member, IEEE,* Weisi Lin, *Senior Member, IEEE,* and Min Liu

Abstract—Proper contrast change can improve the perceptual quality of most images, but it has largely been overlooked in the current research of image quality assessment (IQA). To fill this void, we in this paper first report a new large dedicated contrast-changed image database (CCID2014), which includes 655 images and associated subjective ratings recorded from twenty-two inexperienced observers. We then present a novel reduced-reference image quality metric for contrast change (RIQMC) using phase congruency and statistics information of the image histogram. Validation of the proposed model is conducted on contrast related CCID2014, TID2008, CSIQ and TID2013 databases, and results justify the superiority and efficiency of RIQMC over a majority of classical and state-of-the-art IQA methods. Furthermore, we combine aforesaid subjective and objective assessments to derive the RIQMC based Optimal HIstogram Mapping (ROHIM) for automatic contrast enhancement, which is shown to outperform recently developed enhancement technologies.

Index Terms—Image contrast, subjective / objective quality assessment, statistics information, phase congruency, contrast enhancement, optimal histogram mapping

I. INTRODUCTION

THE requirement of human viewers for high-quality images/videos is constantly increasing at the present time. Broadly speaking, we can define "high quality" as little distortion and appropriate contrast. The former, including commonly encountered blur, noise and compression artifacts, has been deeply explored in existing image quality assessment (IQA) tasks during the last decades, while the latter (contrast change) has been largely overlooked in the literature. We therefore in this paper focus on studying the contrast-changed IQA and the related contrast enhancement technology.

A. Image Quality Assessment

In practice, IQA is an important research topic in image processing, due to its great help for the development of fusion [1], enhancement [2]-[3], and denoising [24]. We can divide IQA into subjective assessment and objective assessment. The first one is generally considered to be the accurate image quality measure, since the human viewer is the ultimate judger

of quality. Nonetheless, subjective methods cannot overcome the drawbacks of being costly and cumbersome, which attracts an increasing number of designs for objective metrics.

Limited by the dependence on subjective image databases [4]-[5], existing objective IQA techniques are mainly devoted to compression, transmission error, noise and blurring artifacts. The two most well-known objective models are perhaps full-reference (FR) peak signal-to-noise ratio (PSNR) and structural similarity index (SSIM) [6], which assume original and distorted image signals are entirely known. Afterwards, many improved SSIM-type of IQA methods have been designed to pursue better performance [7]-[8]. Many FR IQA metrics also came from other models. Visual information fidelity (VIF) [9] is defined from the viewpoint of information measure. Most apparent distortion (MAD) [10] uses the detection- and appearance-based scheme. Realizing the significance of low-level features (e.g. gradient and phase) in the IQA exploration, feature similarity index (FSIM) [11], gradient similarity index (GSIM) [12], internal generative mechanism (IGM) [13], spectral residual (SR) SR-SSIM [14], and VS-based Index (VSI) [15] have been introduced recently.

Reduced-reference (RR) methods work under the situation that the pristine image can be partly available to assist IQA tasks. Note that RR information is restricted to be remarkably smaller than the original image's size. Following Friston's recent discovery of free energy principle [16], we designed the free energy based distortion metric (FEDM) [17] by simulating the internal generative model of the human brain to detect input visual stimuli. Inspired by some observations and analyses on transform domains that have a wide application in image/video processing, RR entropic-difference indexes (RRED) [18] and fourier transform based quality measure (FTQM) [19] were developed independently in discrete wavelet and fourier transform domains. There also exist several RR IQA models through modifying the successful SSIM, e.g. structural degradation model (SDM) [20].

In some cases that the original image signal is unavailable, a growing number of no-reference (NR) methods have been developed under this situation. One type of NR IQA resorts to the help of the support vector machine (SVM) [21] to find the underlying relationship of the chosen features and subjective human ratings, e.g. Distortion Identification-based Image Verity and INtegrity Evaluation (DIIVINE) [22], BLind Image Integrity Notator using DCT Statistics (BLIINDS-II) [23], Blind/Referenceless Image Spatial Quality Evaluator (BRISQUE) [24], and No-reference Free Energy based Robust Metric (NFERM) [25]. Another type of NR methods work even without the employment of human ratings. They include:

K. Gu, G. Zhai and M. Liu are with Institute of Image Communication and Information Processing, Shanghai Jiao Tong University, Shanghai, 200240, China (email: gukesjtuee/guke.doctor@gmail.com; zhaiguangtao@sjtu.edu.cn; liumin_merry@sjtu.edu.cn).

W. Lin is with the School of Computer Engineering, Nanyang Technological University, Singapore 639798 (email: wslin@ntu.edu.sg).

1) natural image quality evaluator (NIQE) [26], measuring the deviations of distorted images from statistical regularities found in natural images; 2) quality-aware clustering (QAC) [27], using a codebook learnt from a group of quality-aware centroids to assess the patches' quality levels for inferring the overall quality index.

Despite the emergence of hundreds of IQA models, very few efforts have been made for the issue of contrast-changed IQA. Therefore, we introduce a new dedicated contrast-changed image database (CCID2014), consisting of 655 images obtained from fifteen natural ones in the Kodak image database [28]. According to the suggestion given by ITU-R BT.500-13 [29], we selected the suitable viewing distance and illuminance, invited 22 inexperienced observers to participate our subjective experiment, and recorded the corresponding mean opinion scores (MOSs) of these viewers.

To solve the problem of subjective IQA in real applications, we further propose a reduced-reference image quality metric for contrast change (RIQMC) using phase congruence (PC) and statistics information of image histogram. We first measure how far the contrast-changed image is from its associated ideal version in entropy, due to its frequent usage in the calculation of the mean unpredictability of an input random variable [30]. Human beings, however, mainly concentrate on salient areas and this enlightens us to estimate the selective entropy on the human concerned regions detected by the PC since mammals perceive features at the areas where the Fourier components are maximal in phase [31].

We also consider the statistical information of crucial meanings in image/video processing and cybernetic systems [32]: 1) the mean (first order statistic) of an image determines the global brightness [33]; 2) the recent optimal contrast-tone mapping (OCTM) provides a new concept of expected context-free contrast defined as the variance (second order statistic) of the histogram [34]; 3) a surface perception model suggests the existence of a connection between the human perception of surface glossiness and the skewness (third order statistics) [35]; 4) several recent studies on natural image analysis reveal that the kurtosis (fourth order statistic) can capture intrinsic properties of natural images [36]. Finally, our RIQMC metric linearly combines the PC based selective entropy and above-mentioned four order statistics of the image histogram, owing to their considerable function in measuring image contrast and characterizing image naturalness.

B. Contrast Enhancement

A direct use of the contrast-changed IQA is enhancement. Histogram equalization (HE) [33] is probably the simplest and broadly applied contrast enhancement technique, which works by redistributing pixel values to effectively flatten and stretch the dynamic range of image histogram, so as to increase the global contrast. But HE easily changes the image luminance and generates undesirable noise/artifacts, leading to excessive enhancement. To deal with these problems, one type of directly modified HE methods aim to preserve the image brightness of the input visual signal [37]-[38].

Another type of technologies is to formulate contrast enhancement as an optimization problem. In [39], Arici *et al.* designed the histogram modification framework (HMF) by first seeking an intermediate histogram $\mathbf{h}$ between the input histogram $\mathbf{h_i}$ and the uniformly distributed histogram $\mathbf{u}$ by minimizing a weighted distance $||\mathbf{h} - \mathbf{h_i}|| + \lambda||\mathbf{h} - \mathbf{u}||$ before performing HE of $\mathbf{h}$. In [34], Wu provided a new definition of image contrast and tone distortion that is solved by the linear programming, and thus proposed the OCTM. In [40], Huang *et al.* presented a simple transformation model via the adaptive gamma correction with weighting distribution (AGCWD). In [41], Raju *et al.* established a fuzzy logic and histogram based method (FLHM) under the control of the mean intensity and the contrast intensification.

Most existing contrast enhancement technologies, however, strongly depend on the manual parameter tuning, and this makes an automatic method highly required. Considering that the positive contrast change can cause valid enhancement, in this research we propose a simple yet effective automatic technique, which uses a quality metric highly correlating with human visual perception to image contrast as the target function and then seeks for the optimal histogram mapping. Two valuable findings in our subjective and objective assessments can help construct the above technique. First, it was viewed from the CCID2014 database that using the proper compound function (mean-shifting followed by logistic function) to transfer the input image can reach the goal of higher image contrast and visual quality, even better than natural images that are often regarded as the perfect. Second, we will confirm that, for each original image and its associated contrast-changed ones, our RIQMC model is able to acquire substantially high performance, and thus can be served as the target function in the search of the optimal histogram mapping. Consequently, we explore the RIQMC based Optimal HIstogram Mapping (ROHIM) for automatic contrast enhancement.

C. The Organization of This Paper

The rest of this paper is organized as follows: Section II first introduces the CCID2014 database and points out the effectiveness of the compound functions for contrast enhancement. In Section III we describe the RR RIQMC algorithms, and in Section IV we compare with numerous classical and state-of-the-art IQA methods on CCID2014, TID2008 [42], CSIQ [43] and TID2013 [44] to confirm the superiority and efficiency of the proposed quality metric. Section V presents our automatic ROHIM enhancement approach, and justifies its effectiveness in comparison to four recently designed models. Finally, Section VI concludes the whole paper.

II. THE CCID2014 IMAGE DATABASE

Part of the CCID2014 database has been roughly provided in a conference paper [45]. In this section, we will describe the entire CCID2014 database. It is known to all that image/video contrast enhancement is a significant and meaningful topic in scientific research and applicational development, in that valid enhancement techniques are capable of improving image/video contrast and visual quality remarkably, even better than the original natural images. Despite of the great advance in the design of quality metrics, the last decade has seen very few

Fig. 1: The fifteen lossless color images in the Kodak database.

Fig. 2: An original image (left) and its transferred image with a suitable compound function (right).

TABLE I: Pre-set points' coordinates for cubic/logistic functions.

Curve & color		p_1	p_2	p_3	p_4
Cubic function	R	$(0,0)$	$(127.5, 127.5)$	$(255, 255)$	$(15, 25)$
	G	$(0,0)$	$(127.5, 127.5)$	$(255, 255)$	$(12, 25)$
	B	$(0,0)$	$(127.5, 127.5)$	$(255, 255)$	$(10, 25)$
	K	$(0,0)$	$(127.5, 127.5)$	$(255, 255)$	$(09, 25)$
Logistic function	R	$(0,0)$	$(127.5, 127.5)$	$(255, 255)$	$(25, 15)$
	G	$(0,0)$	$(127.5, 127.5)$	$(255, 255)$	$(25, 12)$
	B	$(0,0)$	$(127.5, 127.5)$	$(255, 255)$	$(25, 10)$
	K	$(0,0)$	$(127.5, 127.5)$	$(255, 255)$	$(25, 09)$

TABLE II: Subjective experimental conditions and parameters.

Method	Single-stimulus (SS)
Evaluation scales	Continuous quality scale from 1 to 5
Color depth	24-bits/pixel color images
Image coder	Portable Network Graphic (PNG)
Subjects	Twenty-two inexperienced subjects
Image resolution	768×512
Viewing distance	$3 \sim 4$ times the image height
Room illuminance	Dark

papers dedicated to the study of contrast-changed IQA [46]. In fact, none of FR, RR and NR IQA methods has attained satisfactory performance, as reported in the later experiments, and only three small contrast related image subsets in TID2008, CSIQ and TID2013 have been released to the public up to now. To this end, we first present a novel dedicated and more challenging CCID2014 database.

Most of existing image quality databases selected the original images of the same size, in order to eliminate the influence of varying image resolutions. In this research, we therefore chose fifteen representative lossless color images of the size 768×512 from the Kodak image database [28], as given in Fig. 1. The used natural images cover a wide scope of scenes, colors, and foreground/background configurations. Overall 655 images come from an original image $\mathbf{x}$ via the gamma transfer, convex and concave arcs, cubic and logistic functions, the mean-shifting (intensity-shifting), and the compound function (mean-shifting followed by logistic function).

• Gamma transfer: The usual gamma transfer is essentially the power law function, which is defined as $\mathbf{y} = [\mathbf{x} \cdot 255^{(\frac{1}{n}-1)}]^n$, where $n = \{\frac{1}{5}, \frac{1}{3}, \frac{1}{2}, \frac{1}{1.5}, 1.5, 2, 3, 5\}$. We further separate the gamma transfer into two classes: 1) negative gamma transfer for $n \leq 1$; 2) positive gamma transfer for $n > 1$. Figs. 3(a)-(b) give a straightforward illustration of these two classes of gamma transfers.

• Convex and concave arcs: These two arcs are quite similar to the gamma transfer stated above, except each of them is a minor arc of the equal derivative everywhere. We plot them in Figs. 3(c)-(d).

• Cubic and logistic functions: The complicated 3-order cubic function and 4-parameter logistic function are used in this work. The cubic function is defined as

$$\mathbf{y} = F_c(\mathbf{x}, \boldsymbol{a}) = a_1 \cdot \mathbf{x}^3 + a_2 \cdot \mathbf{x}^2 + a_3 \cdot \mathbf{x} + a_4 \quad (1)$$

and the logistic function is given by

$$\mathbf{y} = F_l(\mathbf{x}, \boldsymbol{b}) = \frac{b_1 - b_2}{1 + \exp(-\frac{\mathbf{x}-b_3}{b_4})} + b_2 \quad (2)$$

where $\boldsymbol{a} = \{a_1, ..., a_4\}$ and $\boldsymbol{b} = \{b_1, ..., b_4\}$ are parameters to be determined. Instead of intuitively adjusting the above four parameters in each function, we search for the optimal transfer curve that passes four pre-set points. This optimized process is performed by adopting the "nlinfit" MATLAB function. Since the cubic and logistic functions used in our test are 4-parameter functions, the optimal transfer curve can be solely determined. The pre-set points are listed in Table I, where each group of four pre-set points' coordinates for cubic and logistic functions and R, G, B and K in the second column from left to right separately indicate red, green blue and black curves exhibited in Figs. 3(e)-(f).
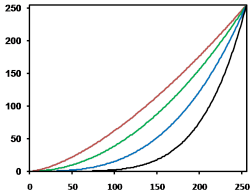
• Mean-shifting: To transfer an original image with 13 levels of $\triangle$ ($= \{0, \pm20, \pm40, \pm60, \pm80, \pm100, \pm120\}$), the mean-shifted image is created by $\mathbf{y} = \mathbf{x} + \triangle$.

• Compound functions: The compound function with mean-shifting followed by logistic transfer is adopted in this study. It stems from an observation that the valid enhancement can be obtained by properly combining mean-shifting and logistic function. For instance, as shown in Fig. 2, the left original image has the lower quality than the right one that is created by using a suitable compound function.

Processed with transfer functions mentioned above, the out of bound values in the produced images were clipped into the range of 0~255. Note that, due to the application of $\triangle = 0$ in the mean-shifting transfer, original images are also included in our CCID2014 database.
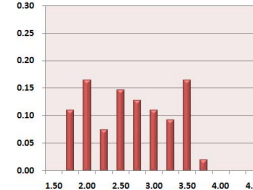
In accordance with ITU-R BT.500-13 [29], we conducted the experiment by using a single-stimulus (SS) method. This subjective test involved 22 inexperienced subjects, most of
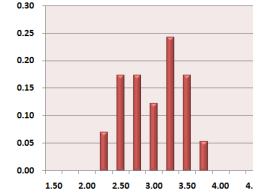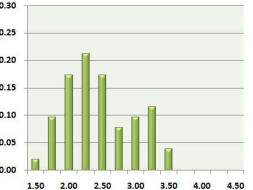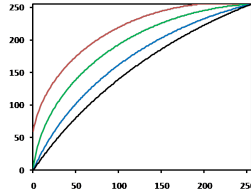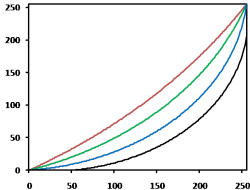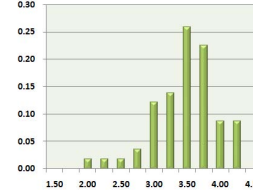
(a) (b) (g) (h) (i)
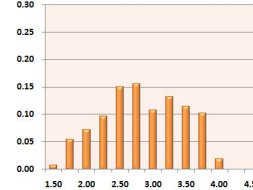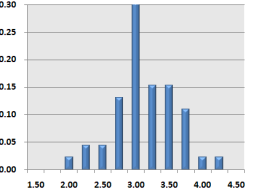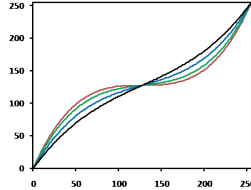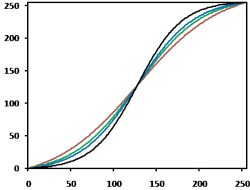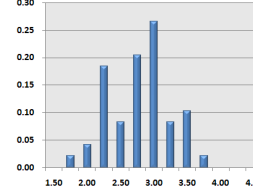
(c) (d) (j) (k) (l)
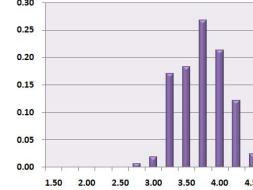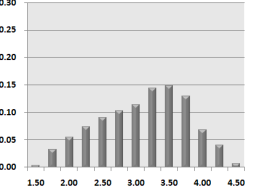
(e) (f) (m) (n) (o)

(I) Illustration of transfer curves   (II) Histograms of MOS values for each image subset

Fig. 3: (I) Illustration of transfer curves: (a) negative gamma transfers; (b) positive gamma transfers; (c) convex arcs; (d) concave arcs; (e) cubic functions; (f) logistic functions. (II) Histograms of MOS values: (g) convex arcs; (h) concave arcs; (i) cubic functions; (j) logistic functions; (k) mean-shifting; (l) negative gamma transfer; (m) positive gamma transfer; (n) compound function; (o) the entire database.

which were college students with various kinds of specialties. We randomized the presentation order of all testing images to reduce memory effects on the mean scores. During assessing the quality of each image, the subjects were required to provide their overall sensation of quality on a continuous quality scale from 1 to 5. We summary major information about the test environment in Table II.

We finally processed all of the gathered MOS values. We assigned s_{cd} as the score obtained from the subject c to the distorted image $\mathbf{y}_d$, where $c = \{1, ..., 22\}$, $d = \{1, ..., 655\}$, before processed the data: 1) Screening the outliers of all observers' ratings caused by inattentive subjects; 2) Computing the MOS score for each image $\mathbf{y}_d$ as $\frac{1}{N_C} \sum_c s_{cd}$, where N_C is the number of participants.

We also plot the distribution of MOS values for different categories of contrast-changed images in Figs. 3 (g)-(o). An important observation in (n) indicate that quite a few images processed by compound functions (i.e. mean-shifting followed by logistic function) have obtained very high subjective quality scores, equal to or larger than 4. In comparison, the MOS values of most original natural images are just around 3.5. We may explain this phenomenon by the fact that the logistic transfer increases the difference of adjacent values' pixels and the complementary mean-shifting adjusts the mean luminance of the input image to be a proper value, especially for natural images [47]. Hence, an appropriate compound function will be considerably helpful for the design of contrast enhancement methods, which will be discussed in Section V.

III. THE PROPOSED RIQMC METRIC

Current IQA researches mainly focus on noise, blur, transmission error, and compression artifacts, and thereby most existing quality metrics were proposed to measure the difference/fidelity between the original and distorted images to predict a quality score. In general, a distorted image has the lower perceptual quality than its corresponding ideal version. Contrast change, however, is distinct from the above distortion types for the reason that an image processed by a proper histogram mapping can obviously improve image contrast and visual quality. Despite the importance of contrast change, most existing IQA models, even state-of-the-art FR quality metrics, work ineffectively for this issue.

As a result, we devote to the IQA of contrast change via a two-stage framework. The first and fundamental stage is to compare the "similarity" of the original and contrast-changed images, since the high-quality image should be not far from its pristine copy. Furthermore, human viewers usually pay attention to salient regions, and this leads us to use the PC to search for the important regions, before estimating the difference of entropy on the selected regions in the original and contrast-changed images. The second stage is related to "comfort". The first and second order statistics (mean and variance) are adopted in this framework inspired by their great contributions in assessing image quality in previous work, e.g. [20] and [25]. The third and fourth order statistics (skewness and kurtosis) are also used according to some recent findings in the neuroscience and natural scene statistics, which reveals
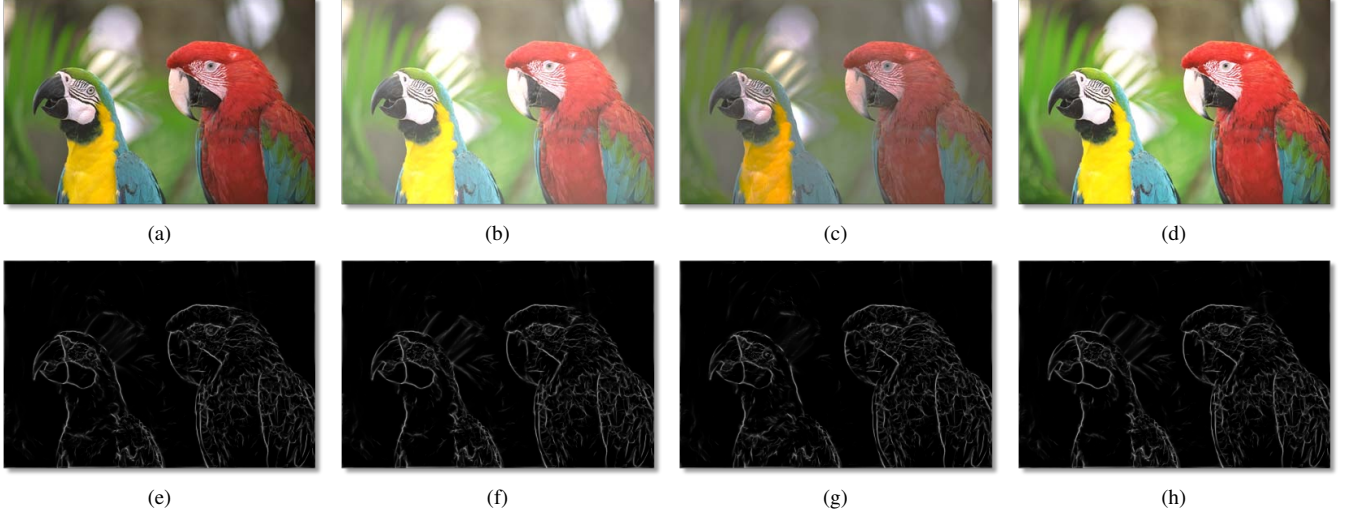
Fig. 4: The top row are an original image "two macaws" (a) and its three contrast-changed versions (b)-(d), while the bottom row are the corresponding PC maps (e)-(h). Though the top row images have clearly different contrast, their PC maps are almost the same.

that high order statistics are connected to the human's feeling of "comfort". At last, we pool the above two parts with a simple linear fusion model to derive the overall quality score.

A. Similarity

Entropy is a chief concept in statistics [30]. It represents the amount of information for a random signal by quantifying its average unpredictability. A high-contrast image is often of large entropy. We first denote the entropy of a contrast-changed image $\mathbf{y}$ as

$$H(\mathbf{y}) = -\sum_{i=0}^{255} P_i(\mathbf{y}) \cdot \log P_i(\mathbf{y}) \tag{3}$$

where $P_i(\mathbf{y})$ indicates the probability density of i-th grayscale in the image $\mathbf{y}$, and $\log(\cdot)$ has base two. Most IQA methods share two steps: 1) local quality/distortion measurement; 2) pooling. As a matter of fact, several efforts have succeeded in estimating perceptual weights for pooling based on singular value decomposition [48], information content [8], and textual connected component [49], and the models have indeed induced noticeable IQA performance gain. This motivates the usage of a proper pooling strategy in this implementation.

Generally, sharp changes in gradient or intensity are used to detect features, whereas the PC theory shows that the Fourier phase rather than the Fourier amplitude stores much more perceptual information in an input visual signal [50], and furthermore, the mammals usually perceive features at those pixels where the Fourier components are maximal in phase. According to the important physiological and psychophysical evidence, a simple yet biologically plausible PC model was defined to detect and identify features in a visual signal [31]. In fact, the PC has been validly incorporated into many IQA techniques [51]-[52].

More precisely, for a signal $\mathbf{s}$, we denote by M_n^e and M_n^o the even- and odd-symmetric filters on scales n, and they form a quadrature pair. Here M_n^e and M_n^o are evaluated using the log-Gabor filters [53]. Responses of each quadrature pair to

the signal will produce a response vector at position j on scale n: $[e_n(j), o_n(j)] = [s(j) * M_n^e, s(j) * M_n^o]$, and the local amplitude on scale n is $A_n(j) = \sqrt{e_n(j)^2 + o_n(j)^2}$. Let $F(j) = \sum_n e_n(j)$ and $H(j) = \sum_n o_n(j)$. The PC can be evaluated by

$$PC(j) = \frac{U(j)}{\varepsilon + \sum_n A_n(j)} \tag{4}$$

where $U(j) = \sqrt{F^2(j) + H^2(j)}$ and ε is a small positive constant for avoiding division by zero. In this paper we apply another easy way to measure the PC [54]:

$$PC(j) = \frac{\sum_n W(j) \lfloor A_n(j) \cdot \Delta\theta_n(j) - T_n \rfloor}{\varepsilon + \sum_n A_n(j)} \tag{5}$$

where $\lfloor \rfloor$ is a floor function rendering the argument unchanged if non-negative, and zero otherwise. T_n indicates an estimate of the noise level. $\Delta\theta_n(j) = \cos[\theta_n(j) - \overline{\theta(j)}] - |\sin[\theta_n(j) - \overline{\theta(j)}]|$ is a sensitive measure of the phase deviation, with $\overline{\theta(j)}$ being the average phase at j. $W(j) = \frac{1}{1 + \exp[(u - t(j))v]}$ is a tapered weighting function, with $t(j) = \frac{\frac{1}{N}\sum_n A_n(j)}{A_{\max}(j) + \varepsilon}$, u being the cut-off value of filter response spread below which PC values become penalized, and v being a gain factor that controls the sharpness of the cutoff. Next, the selective entropy of the contrast-changed image $\mathbf{y}$ is defined as $H_s(\mathbf{y}) = H(\mathbf{y_{pc}})$, where $\mathbf{y_{pc}}$ is constituted by the pixels corresponding to the $l\%$ highest values in the detected PC map.

Despite the fact that entropy measures the average unpredictability of an image signal, it is incapable of characterizing and discriminating various image scenes. For instance, we can easily find out two images that have the same histogram and entropy yet show a beautiful scene and a disorderly picture respectively. Therefore, we compute the difference of selective entropy values of the original and contrast-changed images to measure "similarity". For the original image $\mathbf{x}$, the PC based entropy is similarly defined as $H_s(\mathbf{x})$. We then quantify "similarity" by

$$R_0 = H_s(\mathbf{y}) - H_s(\mathbf{x}). \tag{6}$$

Here we want to emphasize that the two PC maps that are separately computed by applying PC to the pristine image and its contrast-changed version are almost the same, since it is invariant to changes in image brightness or contrast [54]. That is to say, the PC maps computed from different images of the same image content (i.e. the identical original image) are greatly similar. An example in Fig. 4 illustrates this.

B. Comfort

The mean or the first order statistic of $\mathbf{y}$ determines the overall brightness of image histogram. In the photograph technology, a pair of frequently encountered problems are overexposure (high-mean brightness) and underexposure (small-mean brightness), which often degrades the quality of pictures and decreases the comfort of users. Hence, cameras usually have an automatic function of adjusting the image histogram with a possibly suitable gamma transfer. But at the same time, improper selections of gamma functions will instead deteriorate the image contrast and visual quality. So we punish images with very large or low means by introducing a Gaussian kernel to design the first order statistic related term as:

$$R_1 = \exp[-(\frac{E(\mathbf{y}) - \mu}{\nu})^2] \qquad (7)$$

where $E(\mathbf{y})$ is defined as the expectation of the image $\mathbf{y}$, and μ and ν are fixed model parameters of determining the mean and the shape of the used Gaussian kernel.

We can basically categorize early studies of contrast enhancement into two types: context-sensitive and context-free. The former one defines contrast based on the rate of change in intensity between neighboring pixels, and the contrast can be enhanced by directly adjusting the local waveform in a pixel-wise manner. The latter type is to manipulate the input image histogram to separate the gray levels of higher probability further apart from the surrounding gray levels. For example, HE is a classical context-free contrast enhancement technology. Aiming to increase the average difference between any two altered input gray levels, Wu defined a novel concept of expected context-free contrast as a function of variance (second order statistic) of the image histogram recently [34]. Accordingly, we take into account the second order statistic term given by

$$R_2 = \sigma^2(\mathbf{y_h}) = E(\mathbf{y_h^2}) - E(\mathbf{y_h})^2 \qquad (8)$$

where $\mathbf{y_h}$ indicates the histogram of the image $\mathbf{y}$.

In the real life, a great number of common pictures, processed by PS (photoshop) masters, became excellent masterpieces. One of the most important techniques is to adjust the image histogram. In fact, it was found that human viewers use the skewness to assist to make judgements about contrast [35]. For instance, when an image has a positively skewed statistics, it tends to appear darker and glossier than a similar image with lower skewness. Motoyoshi *et al.* provided an interesting surface perception model to explain this phenomenon, which suggests that there exists a connection between the human visual perception to surface glossiness and the skewness (third order statistic). They further simulated a neural mechanism to
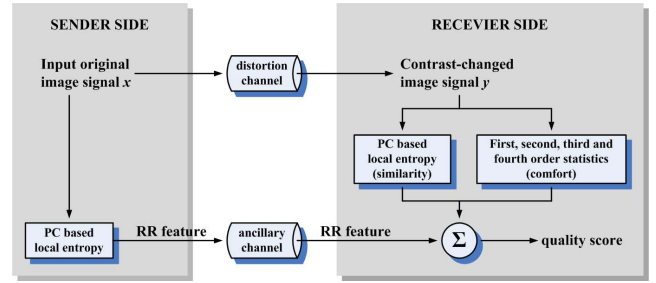

Fig. 5: Illustration of the basic flowchart of our RIQMC metric.

reveal that the on-center and off-center cells and an accelerating nonlinearity in the human visual system compute the subband skewness to estimate the perceptual surface quality. This paper consequently includes the skewness as follows:

$$R_3 = \text{skewness}(\mathbf{y}) = \frac{E[\mathbf{y} - E(\mathbf{y})]^3}{\sigma^3(\mathbf{y})} \qquad (9)$$

where $\sigma(\mathbf{y})$ indicates the image $\mathbf{y}$'s variance value.

The skewness is a measure for the degree of symmetry in the variable distribution, while the higher-order kurtosis is to quantify the degree of peakedness/flatness. In this research, the kurtosis is also used as an index to predict the quality of contrast-changed images. We found that largely skewed images often have tall glossiness, yet they sometimes look unnatural. Based on an observation that the absolute kurtosis value of a contrast-changed image tends to be larger than that of its associated original one, in this paper we thereby adopt the kurtosis as the last term in the RIQMC:

$$R_4 = \text{kurtosis}(\mathbf{y}) = \frac{E[\mathbf{y} - E(\mathbf{y})]^4}{\sigma^4(\mathbf{y})} - 3. \qquad (10)$$

C. Fusion

Finally, we combine the "similarity" and "comfort" together to derive the overall quality scores of contrast-changed images. Here, we use a simple linear fusion to integrate the difference of PC based entropy and four order statistics:

$$\text{RIQMC} = \sum_{i=0}^{4} r_i \cdot R_i$$

$$= \underbrace{- r_0 \cdot H_s(\mathbf{x})}_{\text{For the orignal } \mathbf{x}} + \underbrace{r_0 \cdot H_s(\mathbf{y}) + \sum_{i=1}^{4} r_i \cdot R_i}_{\text{For the contrast-changed } \mathbf{y}} \qquad (11)$$

where r_0 to r_4 are constants of controlling the relative importance of each component. All parameters (l, μ, ν and $r_0, ..., r_4$) are optimized using the contrast related subset in the CSIQ database. Our new database and MATLAB code will be released at http://www.ntu.edu.sg/home/wslin/Publications.htm and https://sites.google.com/site/guke198701/home.

An important note is that our RIQMC model only requires one single number, namely the PC based entropy of the original image $H_s(\mathbf{x})$, as labeled in Eq. (11), which is usually negligible as compared to the image file's size and can be encoded precisely with just a few bits in the header file. For a clear showing, we display the primary flowchart of our technique in Fig. 5.

TABLE III: Performance evaluations of our RIQMC and the testing IQA metrics. We highlight the best two performed approaches.

Metrics	Type	CCID2014 (655 images)				TID2008 (200 images)				CSIQ (116 images)			
		PLCC	SROCC	KROCC	RMS	PLCC	SROCC	KROCC	RMS	PLCC	SROCC	KROCC	RMS
SSIM	FR	0.8256	0.8136	0.6063	0.3689	0.5057	0.4877	0.3402	0.8300	0.7450	0.7397	0.5323	0.1124
MS-SSIM	FR	0.8458	0.8271	0.6236	0.3488	0.6654	0.5877	0.4303	0.7182	0.8959	0.8833	0.6899	0.0748
VIF	FR	**0.8589**	**0.8349**	**0.6419**	**0.3349**	**0.8377**	**0.7879**	**0.5945**	**0.5254**	0.9439	0.9345	0.7775	0.0556
MAD	FR	0.7928	0.7430	0.5458	0.3985	0.3547	0.2828	0.2047	0.8995	0.9321	0.9207	0.7460	0.0610
IW-SSIM	FR	0.8342	0.7811	0.5898	0.3606	0.6996	0.4503	0.3475	0.6874	0.9614	0.9539	0.8168	0.0463
FSIM	FR	0.8183	0.7654	0.5705	0.3758	0.6458	0.4388	0.3331	0.7346	0.9435	0.9421	0.7889	0.0558
GSIM	FR	0.8073	0.7768	0.5711	0.3859	0.6739	0.5126	0.3946	0.7108	0.9325	0.9354	0.7721	0.0608
IGM	FR	0.7806	0.7244	0.5356	0.4087	0.6669	0.4525	0.3272	0.7169	0.9546	0.9547	0.8174	0.0502
SR-SIM	FR	0.7834	0.7363	0.5372	0.4064	0.5995	0.3848	0.2911	0.7701	0.9575	0.9528	0.8165	0.0486
VSI	FR	0.8209	0.7734	0.5735	0.3734	0.6312	0.4571	0.3450	0.7462	0.9533	0.9504	0.8096	0.0509
WASH	FR	0.5689	0.5380	0.3690	0.5378	0.5061	0.3076	0.2051	0.8298	0.8622	0.8412	0.6419	0.0853
FEDM	RR	0.6717	0.5729	0.4073	0.4844	0.6594	0.3228	0.2057	0.7233	**0.9617**	**0.9550**	**0.8189**	**0.0462**
RRED	RR	0.7064	0.6595	0.4677	0.4628	0.5278	0.2320	0.1693	0.8172	0.9415	0.9382	0.7838	0.0568
FTQM	RR	0.7885	0.7292	0.5330	0.4021	0.7530	0.5997	0.4470	0.6331	0.9606	0.9524	0.8129	0.0468
SDM	RR	0.7360	0.6733	0.4862	0.4426	0.7817	0.7378	0.5456	0.6001	0.9175	0.9141	0.7445	0.0670
RIQMC	RR	**0.8726**	**0.8465**	**0.6507**	**0.3194**	**0.8585**	**0.8095**	**0.6224**	**0.4933**	**0.9652**	**0.9579**	**0.8279**	**0.0441**
DIIVINE	NR	0.3664	0.2958	0.2027	0.6084	0.4426	0.3689	0.2552	0.8627	0.4369	0.3958	0.2769	0.1515
BLIINDS-II	NR	0.5862	0.4097	0.2854	0.5298	0.1838	0.0783	0.0563	0.9457	0.1389	0.0989	0.0684	0.1668
BRISQUE	NR	0.3608	0.2165	0.1473	0.6098	0.1535	0.1641	0.1115	0.9507	0.3488	0.2539	0.1706	0.1579
NFERM	NR	0.4074	0.3497	0.2385	0.5691	0.2705	0.2162	0.1472	0.9262	0.4831	0.3742	0.2667	0.1475
NIQE	NR	0.4704	0.3649	0.2489	0.5770	0.0547	0.0588	0.0962	0.9607	0.3019	0.2444	0.1709	0.1606
QAC	NR	0.3072	0.1453	0.0972	0.6223	0.1503	0.0832	0.0534	0.9512	0.3283	0.3187	0.2196	0.1591

Metrics	Type	TID2013 (250 images)				Direct average				Database size-weighted average			
		PLCC	SROCC	KROCC	RMS	PLCC	SROCC	KROCC	RMS	PLCC	SROCC	KROCC	RMS
SSIM	FR	0.5658	0.4905	0.3432	0.8087	0.6605	0.6329	0.4555	0.5300	0.7124	0.6870	0.5018	0.5101
MS-SSIM	FR	0.6476	0.5450	0.4012	0.7474	0.7637	0.7108	0.5362	0.4723	0.7804	0.7355	0.5527	0.4649
VIF	FR	**0.8460**	**0.7720**	**0.5831**	**0.5229**	**0.8716**	**0.8323**	**0.6493**	**0.3597**	**0.8609**	**0.8238**	**0.6350**	**0.3781**
MAD	FR	0.4077	0.3300	0.2558	0.8956	0.6218	0.5691	0.4381	0.5637	0.6554	0.5999	0.4496	0.5503
IW-SSIM	FR	0.6919	0.4528	0.3644	0.7081	0.7968	0.6595	0.5297	0.4506	0.7951	0.6761	0.5255	0.4554
FSIM	FR	0.6578	0.4398	0.3572	0.7388	0.7663	0.6465	0.5125	0.4762	0.7691	0.6620	0.5087	0.4785
GSIM	FR	0.6665	0.4985	0.4024	0.7312	0.7700	0.6808	0.5350	0.4722	0.7685	0.6916	0.5267	0.4789
IGM	FR	0.6715	0.4509	0.3414	0.7268	0.7684	0.6456	0.5054	0.4756	0.7562	0.6458	0.4885	0.4903
SR-SIM	FR	0.6578	0.3917	0.3165	0.7387	0.7496	0.6164	0.4903	0.4909	0.7441	0.6287	0.4782	0.5000
VSI	FR	0.6785	0.4643	0.3705	0.7205	0.7710	0.6613	0.5247	0.4728	0.7733	0.6751	0.5170	0.4749
WASH	FR	0.5182	0.2791	0.1848	0.8388	0.6138	0.4915	0.3502	0.5729	0.5761	0.4761	0.3303	0.6043
FEDM	RR	0.6504	0.3217	0.2373	0.7451	0.7358	0.5431	0.4173	0.4997	0.6929	0.5168	0.3786	0.5353
RRED	RR	0.5606	0.3068	0.2419	0.8122	0.6841	0.5341	0.4157	0.5372	0.6696	0.5438	0.4026	0.5538
FTQM	RR	0.7697	0.6095	0.4685	0.6261	0.8182	0.7229	0.5654	0.4269	0.7953	0.7048	0.5323	0.4520
SDM	RR	0.5831	0.3482	0.2389	0.7968	0.7545	0.6683	0.5038	0.4766	0.7294	0.6402	0.4698	0.5052
RIQMC	RR	**0.8651**	**0.8044**	**0.6178**	**0.4920**	**0.8903**	**0.8546**	**0.6797**	**0.3372**	**0.8775**	**0.8424**	**0.6562**	**0.3571**
DIIVINE	NR	0.4147	0.3034	0.2089	0.8925	0.4151	0.3410	0.2359	0.6288	0.3955	0.3188	0.2196	0.6648
BLIINDS-II	NR	0.0599	0.0390	0.0256	0.9790	0.2422	0.1565	0.1089	0.6553	0.3700	0.2500	0.1741	0.6554
BRISQUE	NR	0.0007	0.0994	0.0685	0.9768	0.2385	0.1835	0.1245	0.6738	0.2704	0.1875	0.1275	0.6978
NFERM	NR	0.2423	0.1956	0.1320	0.9516	0.3535	0.2869	0.1982	0.6548	0.3641	0.3050	0.2090	0.6792
NIQE	NR	0.1659	0.1051	0.0688	0.9672	0.2482	0.1933	0.1306	0.6664	0.3239	0.2501	0.1700	0.6802
QAC	NR	0.1138	0.0304	0.0177	0.9744	0.2249	0.1444	0.0969	0.6768	0.2439	0.1281	0.0853	0.7043

IV. EXPERIMENTAL RESULTS AND ANALYSIS

In this section, we will validate the proposed RIQMC. To the best of our knowledge, four related image databases/subsets (CCID2014, TID2008, CSIQ and TID2013) are used as testing beds. Except our CCID2014 database which has been already described in Section II, the other three are as follows. First, the TID2008 database [42] is a large-scale image quality database, which includes 1,700 images generated from 25 reference images with 17 distortion types at four distortion levels. We choose 200 images corrupted by two distortion types: a) mean shift; b) contrast change. Second, the CSIQ database [43] is composed of totally 866 images, which are created from 30 original counterparts by using six types of distortions at four to five distortion levels. In this research, 116 contrast-changed images are selected for testing. Third, the TID2013 database [44], extended from TID2008, is the largest image database up to now. It contains 25 pristine images and associated 3,000 distorted versions with 24 distortion types at five distortion levels. A total number of 250 images are used here.

Next, our RR RIQMC technique is compared with a large quantity of IQA models: 1) Classical FR SSIM [6], MS-SSIM [7], VIF [9]; 2) Popular FR MAD [10], IW-SSIM [8], FSIM [11], GSIM [12], IGM [13], SR-SIM [14], VSI [15], WASH [55]; 3) RR FEDM [17], RRED [18], FTQM [19], SDM [20]; 4) NR DIIVINE [22], BLIINDS-II [23], BRISQUE [24], NFERM [25], NIQE [26], QAC [27].

On the aforementioned databases, we first map the objective predictions of each quality metric to subjective human ratings using the five-parameter logistic function:

$$q(z) = \beta_1 \left(\frac{1}{2} - \frac{1}{1 + \exp\left(\beta_2 \cdot (z - \beta_3)\right)} \right) + \beta_4 \cdot z + \beta_5 \quad (12)$$

where z and $q(z)$ respectively mean the input score and the mapped score, and β_j $(j = 1, 2, 3, 4, 5)$ are free parameters

TABLE IV: Comparison of average computational time (in second/image) on the overall 655 images in the CCID2014 database.

Model	SSIM	MS-SSIM	VIF	MAD	IW-SSIM	FSIM	GSIM	IGM	SR-SIM	VSI	WASH
Time	0.0685	0.1268	2.4129	2.8079	0.6062	0.6581	0.0392	18.688	0.0636	0.2934	0.2834
Model	FEDM	RRED	FTQM	SDM	RIQMC	DIIVINE	BLIINDS-II	BQISURE	NIQE	NFERM	QAC
Time	86.015	1.5359	0.5912	0.4115	0.8668	24.672	73.591	0.3161	0.4495	43.236	0.1402

TABLE V: Performance comparison with F-test (statistical significance). The symbol "1", "0" or "-1" means that our RIQMC algorithm is statistically (with 95% confidence) better, undistinguishable or worse than the corresponding IQA techniques.

	CCID2014	TID2008	CSIQ	TID2013
SSIM	1	1	1	1
MS-SSIM	1	1	1	1
VIF	1	0	1	0
MAD	1	1	1	1
IW-SSIM	1	1	0	1
FSIM	1	1	1	1
GSIM	1	1	1	1
IGM	1	1	0	1
SR-SIM	1	1	0	1
VSI	1	1	0	1

	CCID2014	TID2008	CSIQ	TID2013
WASH	1	1	1	1
FEDM	1	1	1	1
RRED	1	1	1	1
FTQM	1	1	0	1
SDM	1	1	1	1
DIIVINE	1	1	1	1
BLIINDS-II	1	1	1	1
NIQE	1	1	1	1
NFERM	1	1	1	1
QAC	1	1	1	1

TABLE VI: Monotonicity measures (SROCC) of our RIQMC and serval effective RR and NR IQA methods for each pristine image and its associated contrast-changed versions. We emphasize the best performed algorithm with boldface in each group.

Index	01	02	03	04	05	06	07	08	09	10	11	12	13	14	15
DIIVINE	0.072	0.565	0.307	0.345	0.774	0.673	0.605	0.510	0.620	0.168	0.837	0.695	0.720	0.736	0.596
BRISQUE	0.456	0.129	0.106	0.506	0.077	0.653	0.339	0.028	0.366	0.559	0.664	0.193	0.471	0.853	0.004
NIQE	0.480	0.699	0.322	0.508	0.461	0.561	0.759	0.580	0.694	0.811	**0.860**	0.383	0.398	0.198	0.804
QAC	0.519	0.544	0.041	0.240	0.669	0.162	0.048	0.526	0.081	0.513	0.009	0.055	0.295	0.555	0.375
RRED	0.620	0.665	0.750	0.672	0.722	0.789	0.717	0.756	0.780	0.764	0.724	**0.847**	0.630	0.775	0.532
FTQM	0.600	0.777	**0.811**	0.697	0.739	**0.845**	0.725	0.801	**0.813**	0.728	0.783	0.824	0.698	0.781	0.658
SDM	0.756	0.675	0.362	0.791	0.626	0.549	0.721	0.514	0.623	0.704	0.836	0.703	0.796	0.775	0.765
RIQMC	**0.919**	**0.794**	0.769	**0.842**	**0.805**	0.790	**0.809**	**0.805**	0.807	**0.829**	0.858	0.825	**0.898**	**0.878**	**0.935**

to be determined during the curve fitting process. We then employ four performance measures, as suggested by the video quality experts group (VQEG) [56], to evaluate and compare the proposed metric with those testing IQA models. The first Pearson linear correlation coefficient (PLCC) is computed between subjective MOS/DMOS ratings and the objective scores after nonlinear regression. The second Spearman rank-order correlation coefficient (SROCC) is a non-parametric rank-based correlation metric, independent of any monotonic nonlinear mapping between subjective and objective scores. The third Kendall's rank-order correlation coefficient (KROCC) is another important non-parametric rank correlation metric for measuring the portion of ranks that match between two data sets. And the last root mean-squared (RMS) error is defined as the energy between the converted objective scores and the original ones. In these four performance evaluations, a value close to 1 for PLCC, SROCC and KROCC, yet close to 0 for RMS means superior correlation with subjective ratings.

Table III lists the performance indices of PLCC, SROCC, KROCC and RMS (after the nonlinear regression) and their average results, which is defined as $\bar{\delta} = \sum_{i=1}^{4} \delta_i \cdot w_i / \sum_i w_i$ where δ_i ($i = 1, 2, 3, 4$) is the correlation measure for each of four databases. We set $w_i = 0.25$ for the direct average, while set w_i as the number of images in each database (i.e. 655 for CCID2014, 200 for TID2008, 116 for CSIQ and 250 for TID2013) as the database size-weighted average.

We sum up three advantages of the proposed RIQMC. First, it was found that our RIQMC model, based on the analysis of statistics and phase information, is clearly better than classical and recently designed FR and RR approaches and is also substantially superior to state-of-the-art NR IQA metrics, for contrast-changed contents. It needs to stress that only VIF is matchable with (in fact, a little inferior than) our technique, but it is limited to the FR scenario. Second, the proposed RIQMC is a simple RR IQA model, only composed of several fundamental statistics and phase congruency. It can be conjectured that our approach will be further improved by incorporating other effective operators, such as gradient magnitude that have been broadly used in recent FR IQA tasks [11]-[13]. Besides, we also believe that it will be greatly helpful to insert RIQMC into state-of-the-art IQA metrics, so as to induce their performance gains on the whole CCID2014/TID2008/CSIQ/TID2013 database and contrast related subsets. Third, we want to highlight that the proposed algorithm has very little computational cost. For a direct comparison, we measure the average computational time required to assess an image of size 512×768 (using a computer with Intel i7-2600 processor at 3.40GHz), and report the results in Table IV. It is very obvious that the RIQMC works very efficiently, since it only needs to compute PC maps, entropy and four order statistics.

The statistical significance of the proposed technique is further estimated by the F-test which computes the prediction residuals between the converted objective scores (after the nonlinear mapping) and the subjective ratings. Let F denote the ratio of two residual variances, and $F_{critical}$ (determined
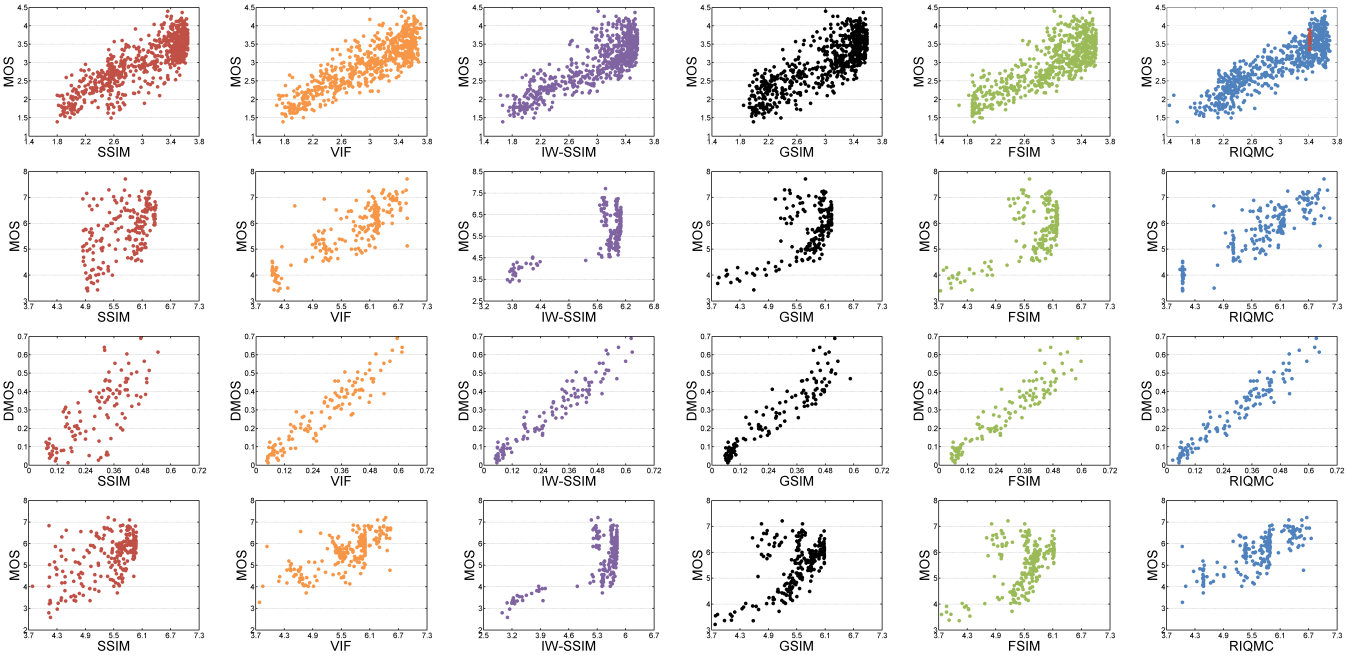
Fig. 6: Scatter plots of MOS/DMOS versus FR classical SSIM, VIF, state-of-the-art IW-SSIM, GSIM, FSIM and our RIQMC model on the databases of CCID2014 (the first row), TID2008 (the second row), CSIQ (the third row) and TID2013 (the fourth row). Red and blue plots in RIQMC (CCID2014) indicate original natural images and their derived contrast-changed copies, respectively.

by the number of residuals and the confidence level) be the judgement threshold. If $F > F_{critical}$, then the difference of prediction between those two metrics is significant. The statistical significance between our algorithm and the other IQA approaches in comparison are listed in Table V, where the symbol "1", "0" or "-1" means that the proposed metric is statistically (with 95% confidence) better, indistinguishable or worse than the corresponding one. It is easy to see that the proposed RIQMC model, despite of the RR nature with only one feature, is statistically better than nearly all of existing classical and state-of-the-art IQA metrics tested in this paper. In particular, our RIQMC is superior to all competing IQA methods on the CCID2014 database.

We also compute the monotonicity of quality predictions between some representative IQA methods and subjective scores on each pristine image and its corresponding contrast-changed counterparts. SROCC is used in our work because it is a significant performance index and has been widely used in quite a few methods for parameter tuning [3], [57]-[58]. Table VI presents the SROCC results, which once again illustrates the effectiveness of our RIQMC model with respect to the testing IQA metrics. Note that most of fifteen SROCC values of RIQMC are higher than 80%.

Finally, we exhibit the scatter plots of MOS/DMOS versus FR classical SSIM, VIF, recent IW-SSIM, GSIM, FSIM, and the proposed RIQMC on four databases in Fig. 6. Clearly, our technique shows higher linearity and monotonicity. Note that adaptive algorithms are more useful in real applications, e.g. segmentation [59]. Seeing the plot of RIQMC on CCID2014, the red and blue plots independently represent the original natural images and their derived contrast-changed versions. Interestingly, we also find that quite a few "blue" contrast-

altered images have higher quality than the "red" ones, which suggests that the quality of natural images is indeed improved by contrast-alteration, and the RIQMC can be used as the target function for contrast enhancement.

V. APPLICATION TO CONTRAST ENHANCEMENT

In Section II we have pointed out that the proper compound function (i.e. mean-shifting followed by logistic transfer) can generate images of better contrast and visual quality. Then we have proposed a new objective IQA method in Section III and demonstrated its superior performance in Section IV. Note that contrast enhancement is a blind process, it requires a NR IQA metric with short execution time in the optimization function to find the optimal histogram mapping:

$$\hat{\mathcal{F}} = \arg\max_{\mathcal{F}} \ \mathcal{T}(\mathcal{F}(\mathbf{x})) \tag{13}$$

where $\mathbf{x}$ is an input image signal, and $\mathcal{F}(\cdot)$ and $\mathcal{T}(\cdot)$ separately indicate the contrast alteration method and NR IQA metric. We can rewrite Eq. (13) to be another equivalent form:

$$\hat{\mathcal{F}} = \arg\max_{\mathcal{F}} \ \mathcal{T}(\mathcal{F}(\mathbf{x})) + c \tag{14}$$

where c is a constant number related to the image content. Since the RR information of our technique for an input image is constant, we can replace the NR IQA metric with RIQMC. On this basis, it is natural to extend the aforesaid subjective and objective assessments to a direct application: automatic contrast enhancement.

A. Automatic Contrast Enhancement

We design the automatic enhancement approach, ROHIM, based on two steps: 1) to adjust the input image histogram

(a) Original   (b) HMF   (c) OCTM   (d) AGCWD   (e) FLHM   (f) ROHIM

Fig. 7: The image "shuttered windows" in the Kodak database and enhanced outputs of HMF, OCTM, AGCWD, FLHM, ROHIM.


(a) Original   (b) HMF   (c) OCTM   (d) AGCWD   (e) FLHM   (f) ROHIM

Fig. 8: The image "five colored hats" in the Kodak database and enhanced outputs of HMF, OCTM, AGCWD, FLHM and ROHIM.

(a) Original   (b) HMF   (c) OCTM   (d) AGCWD   (e) FLHM   (f) ROHIM

Fig. 9: The image "mountain stream" in the Kodak database and enhanced outputs of HMF, OCTM, AGCWD, FLHM, ROHIM.

(a) Original   (b) HMF   (c) OCTM   (d) AGCWD   (e) FLHM   (f) ROHIM
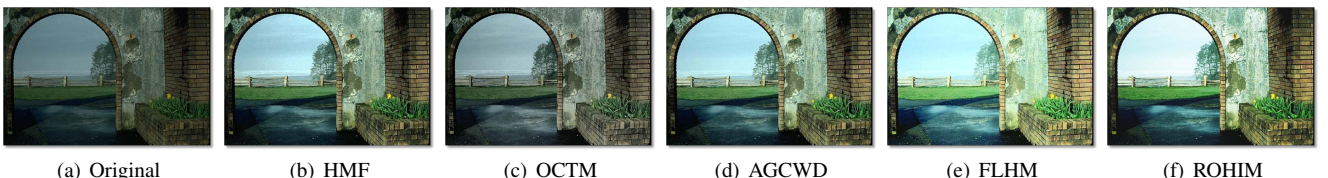
Fig. 10: The image "doorway" in the Berkeley image database and enhanced outputs of HMF, OCTM, AGCWD, FLHM, ROHIM.

using the compound function; 2) to find the optimal parameters maximizing the target function RIQMC. To specify, we first apply mean-shifting function to alter $\mathbf{x}$:

$$\mathbf{x}' = \mathbf{x} + \phi \qquad (15)$$

where ϕ is to be determined by the subsequent optimization operation. We further use the logistic function as follows:

$$\mathbf{y} = F_l(\mathbf{x}', \boldsymbol{\xi}) \qquad (16)$$

where $F_l(\cdot)$ was given in Eq. (2). Note that directly controlling $\boldsymbol{\xi} = \{\xi_1, \xi_2, \xi_3, \xi_4\}$ is very hard because we are not very clear what function these four parameters should take. Therefore we indirectly manipulate the parameter $\boldsymbol{\xi}$ and the function $F_l(\cdot)$ by setting four pairs of pixel values (s_i, t_i) to fix the logistic function. In this implementation we set $s_i = t_i$ ($i = 1...3$) for simplicity. Thus, $\boldsymbol{\xi} = \{\xi_1, \xi_2, \xi_3, \xi_4\}$ can be calculated by minimizing

$$\hat{\boldsymbol{\xi}} = \arg\min_{\boldsymbol{\xi}} \sum_{i=1}^{4} \left| t_i - F_l(s_i, \boldsymbol{\xi}) \right|$$

$$\text{subject to} \quad s_i = t_i \quad \text{when} \ i = 1, ..., 3. \qquad (17)$$

For an easy convergence in the following optimization, the parameter ϕ is initialized as $L - \text{mean}(\mathbf{x})$ (L is defined as the half of the maximum dynamic range of the input image) and the initial values of (s_i, t_i) can be set as the values in the G row of logistic function in Table I. We further demand

$\{s_1, ..., s_4\}$ and $\{t_1, ..., t_3\}$ unchanged and leave only two variables $\{t_4, \phi\}$ to be free parameters, in order to make the optimization process work efficiently.

Next, we adjust $\{t_4, \phi\}$ to transfer a raw image and find the optimal solution of $\{t_4, \phi_{opt}\}$ and the associated $\boldsymbol{\xi}_{opt}$ output with the simplex method, by searching for the optimal transferred image of the maximal RIQMC score. We finally create the enhanced image $\mathbf{y}_{opt}$ via the optimal transfer mapping that combines mean-shifting and logistic functions based on ϕ_{opt} and $\boldsymbol{\xi}_{opt}$:

$$\mathbf{y}_{opt} = \max\{\min[F_l(\mathbf{x} + \phi_{opt}, \boldsymbol{\xi}_{opt}), 255], 0\} \qquad (18)$$

where max and min operators are used to maintain $\mathbf{y}_{opt}$ in the bound values of $0 \sim 255$.

B. Performance Comparison

We pick some images of various scenes and colors from Kodak [28] and Berkeley [60], including "shuttered windows", "five colored hats", "mountain stream", "doorway", "water rafters", "Head light", "mountain chalet", and "wild yak". We show the above images in Figs. 7-14(a), and their enhanced results of HMF, OCTM, AGCWD, FLHM and our ROHIM in Figs. 7-14(b)-(e). It is easy to find that HMF [39] seeks the tradeoff between the input image and its HE image. As indicated in Figs. 7-9, 11, 14(b), HMF improves the contrast of input visual signals, but they look a little dim. We also

(a) Original   (b) HMF   (c) OCTM   (d) AGCWD   (e) FLHM   (f) ROHIM

Fig. 11: The image "water rafters" in the Kodak database and enhanced outputs of HMF, OCTM, AGCWD, FLHM and ROHIM.

(a) Original   (b) HMF   (c) OCTM   (d) AGCWD   (e) FLHM   (f) ROHIM
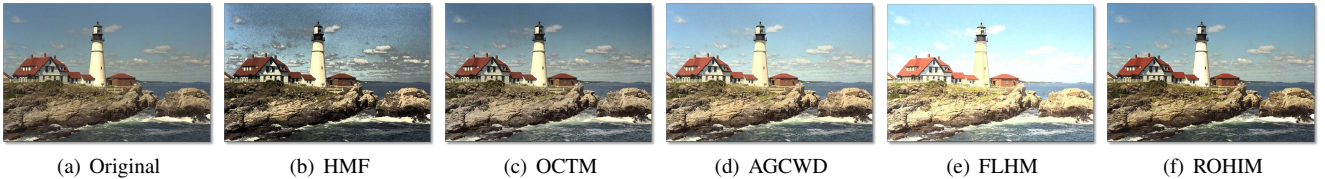
Fig. 12: The image "Head light" in the Kodak image database and enhanced outputs of HMF, OCTM, AGCWD, FLHM, ROHIM.

(a) Original   (b) HMF   (c) OCTM   (d) AGCWD   (e) FLHM   (f) ROHIM
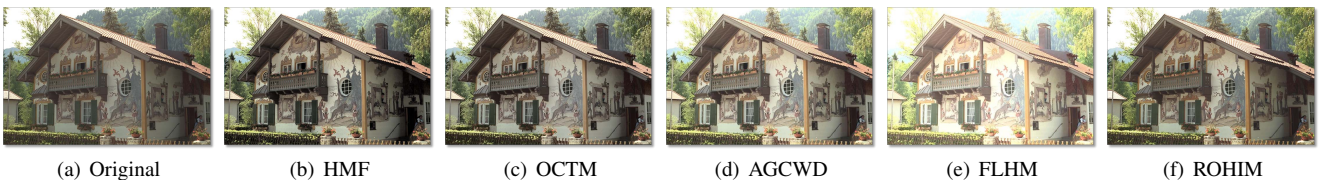
Fig. 13: The image "mountain chalet" in the Kodak database and enhanced outputs of HMF, OCTM, AGCWD, FLHM, ROHIM.

(a) Original   (b) HMF   (c) OCTM   (d) AGCWD   (e) FLHM   (f) ROHIM
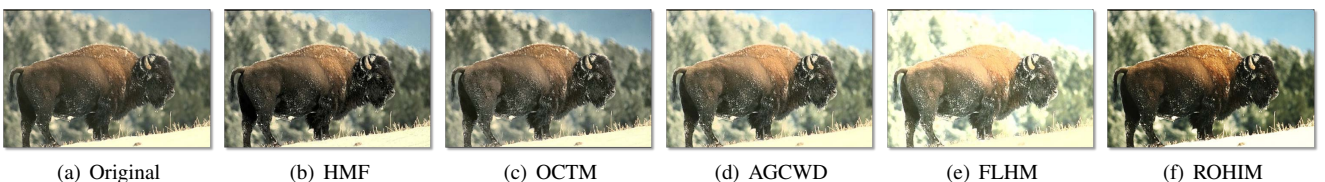
Fig. 14: The image "wild yak" in the Berkeley image database and enhanced outputs of HMF, OCTM, AGCWD, FLHM, ROHIM.

note that Fig. 12(b) has obvious noise. That is to say, HMF cannot provide proper brightness and cannot totally overcome the noise injection.

OCTM [34] works by first providing a novel definition of image contrast and tone distortion, then using this definition to formulate contrast enhancement as an optimization function, and finally solving the optimization problem with linear programming. As shown in Figs. 7-14(c), OCTM solves the problem of noise introduction and its enhanced outputs have been improved better than the inputs. However, we also observe that the enhanced images created by OCTM look quite dull and pale.

AGCWD [40] is based on a simple transformation of the adaptive gamma correction with weighting distribution. It is not difficult to find in Figs. 7-14(d) that AGCWD is able to well restrain the generation of noise artifacts, whereas it is not good at adjusting luminance, making enhanced images overly bright in most cases.

FLHM [41] is built upon the fuzzy logic and histogram under the control of two parameters, one the mean intensity and the other the contrast intensification. As can be seen in Fig. 10(e), FLHM is well suited for enhancement of low contrast images, but not good at advancing the visual quality of natural images, as given in Figs. 7-9(e), 11-14(e).

ROHIM is proposed by fusing subjective and objective quality assessments for image contrast. In comparison to the above

four, our approach effectively avoids artifacts and preserve details, and furthermore, it makes enhanced images of more suitable luminance and glossier than state-of-the-art HMF, OCTM and AGCWD techniques. A reasonable explanation of this phenomenon is that the proposed ROHIM model first uses the logistic transfer to augment the difference of adjacent pixel values and uses the mean shifting to alter the input image to be of an appropriate luminance, and then uses the high-accuracy RIQMC, which well correlates with human perception to the quality of contrast-changed images, to find the best fusion of logistic and mean-shifting functions.

A quantitative comparison between different enhancement algorithms is also conducted. We invited 50 viewers (38 males and 12 females) to score the overall enhanced images in Figs. 7-14 by the popular paired comparison method. Particularly, for each group of six images (including the original image and enhanced images by HMF, OCTM, AGCWD, FLHM and ROHIM), the participants will give their opinions for a total of 15 image pairs, in order to decide which is better between a pair of images. We sum up the winning times for each image and their averages across eight testing images, as tabulated in Table VII. Higher score means better performance. Results of experiments tell that our enhancement technique outperforms the algorithms tested, and furthermore, the proposed ROHIM model has won the first place on all image sets.

TABLE VII: Subjective opinion scores of images in Figs. 7-14 and their average scores for each contrast enhancement technique. We highlight the best performed algorithm with boldface.

j-th	ORG	HMF	OCTM	AGCWD	FLHM	ROHIM
1	139	114	113	135	40	**209**
2	107	146	114	134	60	**189**
3	95	158	119	144	50	**184**
4	67	127	81	147	135	**193**
5	94	163	153	118	28	**194**
6	146	38	115	162	75	**214**
7	122	157	111	91	54	**215**
8	100	151	128	140	27	**204**
Mean	109	132	117	134	59	**200**

VI. CONCLUSION

In this paper we have examined the problem of IQA for contrast change and the related application to automatic image enhancement. Three main contributions have been made in our study. First, we build a carefully-designed and dedicated contrast-changed image database (CCID2014) to facilitate the research of contrast-changed IQA. This database includes 655 images created by various kinds of contrast-oriented transfer functions, consisting of gamma transfer, concave and convex arcs, cubic and logistic functions, mean-shift and compound functions (mean-shifting followed by logistic function), and associated MOS values scored by 22 inexperienced observers. Second, we further develop a high-performance RR RIQMC metric by combining two respects of measures in "similarity" and "comfort". The proposed RIQMC is superior to classical and state-of-the-art FR, RR and NR IQA methods on contrast related CCID2014, TID2008, CSIQ, and TID2013 databases, and furthermore, it only requires very little RR information (a single number of PC based entropy of the original image) and short computational time. Third, we present an automatic contrast enhancement ROHIM model using subjective and objective assessments for image contrast, which can enhance images better than recent enhancement technologies.

REFERENCES

[1] L. Snidaro, R. Niu, G. L. Foresti, and P. K. Varshney, "Quality-based fusion of multiple video sensors for video surveillance," *IEEE Trans. Syst., Man, Cybern. B, Cybern.*, vol. 37, no. 4, pp. 1044-1051, Aug. 2007.

[2] K. Panetta, S. S. Agaian, Y. Zhou, and E. J. Wharton, "Parameterized logarithmic framework for image enhancement," *IEEE Trans. Syst., Man, Cybern. B, Cybern.*, vol. 41, no. 2, pp. 460-473, Apr. 2011.

[3] K. Gu, G. Zhai, X. Yang, W. Zhang, and C. W. Chen, "Automatic contrast enhancement technology with saliency preservation," *IEEE Trans. Circuits Syst. Video Technol.*, vol. 25, 2015.

[4] W. Lin and C.-C. Jay Kuo, "Perceptual visual quality metrics: A survey," *J. Vis. Commun. Image Represent.*, vol. 22, no. 4, pp. 297-312, May 2011.

[5] K. Gu, G. Zhai, X. Yang, and W. Zhang, "Hybrid no-reference quality metric for singly and multiply distorted images," *IEEE Trans. Broadcasting*, vol. 60, no. 3, pp. 555-567, Sept. 2014.

[6] Z. Wang, A. C. Bovik, H. R. Sheikh, and E. P. Simoncelli, "Image quality assessment: From error visibility to structural similarity," *IEEE Trans. Image Process.*, vol. 13, no. 4, pp. 600-612, Apr. 2004.

[7] Z. Wang, E. P. Simoncelli, and A. C. Bovik, "Multi-scale structural similarity for image quality assessment," *in Proc. IEEE Asilomar Conf. Signals, Syst., Comput.*, pp. 1398-1402, Nov. 2003.

[8] Z. Wang and Q. Li, "Information content weighting for perceptual image quality assessment," *IEEE Trans. Image Process.*, vol. 20, no. 5, pp. 1185-1198, May 2011.

[9] H. R. Sheikh, and A. C. Bovik, "Image information and visual quality," *IEEE Trans. Image Process.*, vol. 15, no. 2, pp. 430-444, Feb. 2006.

[10] E. C. Larson, and D. M. Chandler, "Most apparent distortion: Full-reference image quality assessment and the role of strategy," *Journal of Electronic Imaging*, vol. 19, no. 1, Jan. 2010.

[11] L. Zhang, L. Zhang, X. Mou, and D. Zhang, "FSIM: A feature similarity index for image quality assessment," *IEEE Trans. Image Process.*, vol. 20, no. 8, pp. 2378-2386, Aug. 2011.

[12] A. Liu, W. Lin, and M. Narwaria, "Image quality assessment based on gradient similarity," *IEEE Trans. Image Process.*, vol. 21, no. 4, pp. 1500-1512, Apr. 2012.

[13] J. Wu, W. Lin, G. Shi, and A. Liu, "Perceptual quality metric with internal generative mechanism," *IEEE Trans. Image Process.*, vol. 22, no. 1, pp. 43-54, Jan. 2013.

[14] L. Zhang and H. Li, "SR-SIM: A fast and high performance IQA index based on spectral residual," *in Proc. IEEE Int. Conf. Image Process.*, pp. 1473-1476, Sept. 2012.

[15] L. Zhang, Y. Shen, and H. Li, "VSI: A visual saliency induced index for perceptual image quality assessment," *IEEE Trans. Image Process.*, vol. 23, no. 10, pp. 4270-4281, Oct. 2014.

[16] K. Friston, "The free-energy principle: A unified brain theory?" *Nature Reviews Neuroscience*, vol. 11, pp. 127-138, 2010.

[17] G. Zhai, X. Wu, X. Yang, W. Lin, and W. Zhang, "A psychovisual quality metric in free-energy principle," *IEEE Trans. Image Process.*, vol. 21, no. 1, pp. 41-52, Jan. 2012.

[18] R. Soundararajan and A. C. Bovik, "RRED indices: Reduced-reference entropic differencing for image quality assessment," *IEEE Trans. Image Process.*, vol. 21, no. 2, pp. 517-526, Feb. 2012.

[19] M. Narwaria, W. Lin, I. V. McLoughlin, S. Emmanuel, and L. T. Chia, "Fourier transform-based scalable image quality measure," *IEEE Trans. Image Process.*, vol. 21, no. 8, pp. 3364-3377, Aug. 2012.

[20] K. Gu, G. Zhai, X. Yang, and W. Zhang, "A new reduced-reference image quality assessment using structural degradation model," *in Proc. IEEE Int. Symp. Circuits and Systems*, pp. 1095-1098, May 2013.

[21] C-C. Chang and C-J. Lin, "LIBSVM: a library for support vector machines," *ACM Trans. Intelligent Systems and Technology*, vol. 2, no. 3, 2011. Software available at http://www.csie.ntu.edu.tw/~cjlin/libsvm.

[22] A. K. Moorthy and A. C. Bovik, "Blind image quality assessment: From scene statistics to perceptual quality," *IEEE Trans. Image Process.*, pp. 3350-3364, vol. 20, no. 12, Dec. 2011.

[23] M. A. Saad, A. C. Bovik, and C. Charrier, "Blind image quality assessment: A natural scene statistics approach in the DCT domain," *IEEE Trans. Image Process.*, pp. 3339-3352, vol. 21, no. 8, Aug. 2012.

[24] A. Mittal, A. K. Moorthy, and A. C. Bovik, "No-reference image quality assessment in the spatial domain," *IEEE Trans. Image Process.*, pp. 4695-4708, vol. 21, no. 12, Dec. 2012.

[25] K. Gu, G. Zhai, X. Yang, and W. Zhang, "Using free energy principle for blind image quality assessment," *IEEE Trans. Multimedia*, vol. 17, no. 1, pp. 50-63, Jan. 2015.

[26] A. Mittal, R. Soundararajan, and A. C. Bovik, "Making a 'completely blind' image quality analyzer," *IEEE Signal Processing Letters*, pp. 209-212, vol. 22, no. 3, Mar. 2013.

[27] W. Xue, L. Zhang, and X. Mou, "Learning without human scores for blind image quality assessment," *in Proc. IEEE Int. Conf. Computer Vision and Pattern Recognition*, pp. 995-1002, Jun. 2013.

[28] Kodak Lossless True Color Image Suite: http://r0k.us/graphics/kodak/

[29] Methodology for the subjective assessment of the quality of television pictures. International Telecommunication Union Recommendation ITU-R BT.500-13, 2012.

[30] C. E. Shannon, "A mathematical theory of communication," *Bell Syst. Tech. J.*, vol. 27, pp. 379-423, Oct. 1948.

[31] M. C. Morrone, J. Ross, D. C. Burr, and R. Owens, "Mach bands are phase dependent," *Nature*, vol. 324, no. 6049, pp. 250-253, Nov. 1986.

[32] H. Zhang, J. Yang, Y. Zhang, and T. S. Huang, "Image and video restorations via nonlocal kernel regression," *IEEE Trans. Cybernetics*, vol. 43, no. 3, pp. 1035-1046, Jun. 2013.

[33] R. C. Gonzalez and R. E. Woods, Digital Image Processing. Addison-Wesley, Reading, MA, 1992.

[34] X. Wu, "A linear programming approach for optimal contrast-tone mapping," *IEEE Trans. Image Process.*, vol. 20, no. 5, pp. 1262-1272, May 2011.

[35] I. Motoyoshi, S. Nishida, L. Sharan, and E. H. Adelson, "Image statistics and the perception of surface qualities," *Nature*, vol. 447, pp. 206-209, May 2007.

[36] D. Zoran and Y. Weiss, "Scale invariance and noise in natural images," *in Proc. IEEE Int. Conf. Comput. Vis.*, pp. 2209-2216, 2009.

[37] Y. T. Kim, "Contrast enhancement using brightness preserving bi-histogram equalization," *IEEE Trans. Consumer Electron.*, vol. 43, no. 1, pp. 1-8, Feb. 1997.

[38] Y. Wang, Q. Chen, and B. Zhang, "Image enhancement based on equal area dualistic sub-image histogram equalization method," *IEEE Tran. Consumer Electron.*, vol. 45, no. 1, pp. 68-75, Feb. 1999.

[39] T. Arici, S. Dikbas, and Y. Altunbasak, "A histogram modification framework and its application for image contrast enhancement," *IEEE Trans. Image Process.*, vol. 18, no. 9, pp. 1921-1935, Sept. 2009.

[40] S.-C. Huang, F.-C. Cheng, and Y.-S. Chiu, "Efficient contrast enhancement using adaptive gamma correction with weighting distribution," *IEEE Trans. Image Process.*, pp. 1032-1041, vol. 22, no. 3, Mar. 2013.

[41] G. Raju and M. S. Nair, "A fast and efficient color image enhancement method based on fuzzy-logic and histogram," *Int. J. Electronics and Communications*, vol. 68, no. 3, pp. 237-243, Mar. 2014.

[42] N. Ponomarenko *et al.*, "TID2008-A database for evaluation of full-reference visual quality assessment metrics," *Advances of Modern Radioelectronics*, vol. 10, pp. 30-45, 2009.

[43] E. C. Larson and D. M. Chandler, "Categorical image quality (CSIQ) database," [Online], Available: http://vision.okstate.edu/csiq

[44] N. Ponomarenko *et al.*, "Image database TID2013: Peculiarities, results and perspectives," *Sig. Process.: Image Commun.*, vol. 30, pp. 57-55, Jan. 2015.

[45] K. Gu, G. Zhai, X. Yang, W. Zhang, and M. Liu, "Subjective and objective quality assessment for images with contrast change," *in Proc. IEEE Int. Conf. Image Process.*, pp. 383-387, Sept. 2013.

[46] W. Lin, L. Dong, and P. Xue, "Visual distortion gauge based on discrimination of noticeable contrast changes," *IEEE Trans. Circuits Syst. Video Technol.*, vol. 15, no. 7, pp. 900-909, Jul. 2005.

[47] V. Mante, R. A Frazor, V. Bonin, W. S Geisler, and M. Carandini, "Independence of luminance and contrast in natural scenes and in the early visual system," *Nature neuroscience*, vol. 8, no. 12, pp. 1690-1697, Dec. 2005.

[48] M. Narwaria and W. Lin, "SVD-based quality metric for image and video using machine learning," *IEEE Trans. Syst., Man, Cybern. B, Cybern.*, vol. 42, no. 2, pp. 347-364, Apr. 2012.

[49] H. Yang, S. Wu, C. Deng, and W. Lin, "Scale and orientation invariant text segmentation for born-digital compound images," *IEEE Trans. Cybern.*, vol. 45, no. 3, pp. 533-547, Mar. 2015.

[50] A. V. Oppenheim and J. S. Lim, "The importance of phase in signals," *Proc. IEEE*, vol. 69, no. 5, pp. 529-541, Nov. 1981.

[51] C. Li, A. C. Bovik, and X. Wu, "Blind image quality assessment using a general regression neural network," *IEEE Trans. Neural Networks*, vol. 22, no. 5, pp. 793-399, May 2011.

[52] C. Li, Y. Ju, A. C. Bovik, X. Wu, and Q. Sang, "No-training, no-reference image quality index using perceptual features," *Optical Engineering*, vol. 52, no. 5, May 2013.

[53] D. J. Field, "Relations between the statistics of natural images and the response properties of cortical cells," *J. Opt. Soc. Amer. A*, vol. 4, no. 12, pp. 2379-2394, 1987.

[54] P. Kovesi, "Image features from phase congruency," *Videre: J. Comp. Vis. Res.*, vol. 69, no. 3, pp. 1-26, 1999.

[55] M. Reenu, D. Dayana, S. S. A. Raj, and M. S. Nair, "Wavelet based sharp features (WASH): An image quality assessment metric based on HVS," *in Proc. IEEE Int. Conf. Advanced Computing, Networking and Security*, pp. 79-83, Dec. 2013.

[56] VQEG, "Final report from the video quality experts group on the validation of objective models of video quality assessment," Mar. 2000, http://www.vqeg.org/.

[57] C. Li and A. C. Bovik, "Content-partitioned structural similarity index for image quality assessment," *Signal Processing: Image Communication*, vol. 25, no. 7, pp. 517-526, Aug. 2010.

[58] K. Gu, G. Zhai, X. Yang, and W. Zhang, "A new psychovisual paradigm for image quality assessment: From differentiating distortion types to discriminating quality conditions," *Signal, Image and Video Processing*, vol. 7, no. 3, pp. 423-436, May 2013.

[59] B. Wang, X. Gao, D. Tao, and X. Li, "A nonlinear adaptive level set for image segmentation," *IEEE Trans. Cybernetics*, vol. 44, no. 3, pp. 418-428, Mar. 2014.

[60] D. Martin, C. Fowlkes, D. Tal, and J. Malik, "A database of human segmented natural images and its application to evaluating segmentation algorithms and measuring ecological statistics," *in Proc. IEEE Int. Conf. Comput. Vis.*, pp. 416-423, 2001.

Ke Gu received the B.S. degree in electronic engineering from Shanghai Jiao Tong University, Shanghai, China, in 2009. He is currently working toward the Ph.D. degree. He is the reviewer for some IEEE Transactions and Journals, including IEEE Transactions on Cybernetics, IEEE Signal Processing Letters, Neurocomputing, Journal of Visual Communication and Image Representation, and Signal, Image and Video Processing.

From July to November 2014, he was a visiting student at the Department of Electrical and Computer Engineering, University of Waterloo, Canada. From December 2014 to January 2015, he was a visiting student at the School of Computer Engineering, Nanyang Technological University, Singapore. His research interests include quality assessment and contrast enhancement.

Guangtao Zhai (M'10) received the B.E. and M.E. degrees from Shandong University, Shandong, China, in 2001 and 2004, respectively, and the Ph.D. degree from Shanghai Jiao Tong University, Shanghai, China, in 2009, where he is currently a Research Professor with the Institute of Image Communication and Information Processing.

From 2008 to 2009, he was a Visiting Student with the Department of Electrical and Computer Engineering, McMaster University, Hamilton, ON, Canada, where he was a Post-Doctoral Fellow from 2010 to 2012. From 2012 to 2013, he was a Humboldt Research Fellow with the Institute of Multimedia Communication and Signal Processing, Friedrich Alexander University of Erlangen-Nuremberg, Germany. He received the Award of National Excellent Ph.D. Thesis from the Ministry of Education of China in 2012. His research interests include multimedia signal processing and perceptual signal processing.

Weisi Lin (M'92-SM'98) received the Ph.D. degree from Kings College, London University, London, U.K., in 1993.

He is currently an Associate Professor with the School of Computer Engineering, Nanyang Technological University, and served as a Lab Head of Visual Processing, Institute for Infocomm Research. He authors over 300 scholarly publications, holds 7 patents, and receives over S$ 4 million in research grant funding. He has maintained active long-term working relationship with a number of companies. His research interests include image processing, video compression, perceptual visual and audio modeling, computer vision, and multimedia communication.

He served as an Associate Editor of IEEE Transactions on Multimedia, IEEE Signal Processing Letters, and Journal of Visual Communication and Image Representation. He is also on six IEEE Technical Committees and Technical Program Committees of a number of international conferences. He was the Lead Guest Editor for a special issue on perceptual signal processing of the IEEE Journal OF Selected Topics in Signal Processing in 2012. He is a Chartered Engineer in the U.K., a fellow of the Institution of Engineering Technology, and an Honorary Fellow of the Singapore Institute of Engineering Technologists. He Co-Chaired the IEEE Multimedia Communications Technical Committee (MMTC) special interest group on quality of experience. He was an Elected Distinguished Lecturer of APSIPA in 2012/3.

Min Liu received the B.E. degree in electronic engineering from Xidian University, Xian, China, in 2012. She is currently working toward the Ph.D. degree in Shanghai Jiao Tong University. Her research interests include image/video quality assessment and perceptual signal processing.